Hindawi Publishing Corporation
Research Letters in Physics
Volume 2008, Article ID 148505, 5 pages
doi:10.1155/2008/148505

Research Letter

Nanopinholes-Based Optical Superlens

Yongqi Fu,[1] Chunlei Du,[1] Wei Zhou,[2] and Lennie Enk Ng Lim[2]

[1] *State Key Laboratory of Optical Technologies for Microfabrication, Institute of Optics and Electronics, Chinese Academy of Sciences, Chengdu 610209, China*
[2] *Precision Engineering and Nanotechnology Centre, School of Mechanical and Aerospace Engineering, Nanyang Technological University, 50 Nanyang Avenue, Singapore 639798*

Correspondence should be addressed to Yongqi Fu, yqfu@ioe.ac.cn

Received 10 October 2007; Accepted 3 January 2008

Recommended by Nathan Ida

A type of nanopinhole-based plasmonic structure is presented. It can realize superfocusing within micron-scale propagation distance with spatial resolution beyond diffraction limit. Cut-off wavelength effect is highlighted for understanding how periodicity distribution of the nanopinholes influences transmission and focusing through the structure. Redshift peak transmission occurs while the periodicity increases. In addition, focusing property of the plasmonic structures is analyzed for the monochromatic illumination with different incident wavelengths ranging from 400 nm to 750 nm. The easy fabrication and high focusing performance of the proposed structures may be used in data storage devices, bioimaging, and nanolithography.

Photon sieves are a type of diffractive optical elements (DOEs) developed for soft X-ray focusing and imaging. Spatial resolution of the conventional diffractive lenses, such as Fresnel zone plate, is in the order of the width of the outmost zone [1–3]. Therefore, reducing feature size of the zone plates helps to improve the spatial resolution. Unfortunately, however, the smallest feature sizes which can be fabricated by means of today's lithographic techniques are typically in the range of 20 nm to 40 nm. To overcome the limitation in resolution, Kipp et al. [4] put forth in 2001 a new type of DOE, which was referred to as photon sieves. Relevant theoretical analyses and applications have been reported consequently regarding the photon sieves [5–11]. All the photon sieves reported so far work in far-field region with macroscale dimensions and their minimum hole diameter is larger than the incident wavelength λ. If the pinhole diameter could be made smaller than $\lambda/2$ in a homogeneous dielectric material, then cut-off wavelength effect would occur. Therefore, we put forth a nanostructure which is composed of pinholes with micron-scale dimension and diameter smaller than $\lambda/2$. We refer to this structure as nanopinhole-based plasmonic structure (NPPS) and explore its application as "superlens." Influence of the cut-off wavelength effect on propagation and transmission properties is analyzed for the purpose of revealing optical performance and physical picture of the structure in near-field region.

Our proposed superlens is an asymmetric structure in which a thin film of Ag of 200 nm in thickness is sandwiched between air and quartz substrate. The pinholes with different diameters are uniformly and symmetrically distributed along the open subwavelength zones of a zone plate. It works at visible wavelength regime and propagates at near field with the outer diameter $D < 15\,\mu$m and zone number $N < 10$.

The size of a given hole is a factor K which is larger than the corresponding zone width of a zone plate having the same diameter and focal length. K is chosen to maximize the field contribution at the focus [10]. For the conventional photo sieves with the smallest pinhole diameters larger than the incident wavelength λ_{in}, the focal beam spot size is smaller than the diameter of the outmost pinholes by the factor K. However, for our pinholes with diameters much smaller than λ_{in}, there exists a cut-off wavelength λc. For a plane wave illumination at normal incidence with $E_{\parallel}$ field, the cut-off wavelength effect occurs in case the pinhole diameter d is equal to $\lambda/2$, that is, when $\lambda = 2d$. For the wavelengths longer than $2d$, $|E|^2$ decays exponentially because the light beaming at these wavelengths cannot propagate within the holes [12]. However, for the plane wave illumination with component

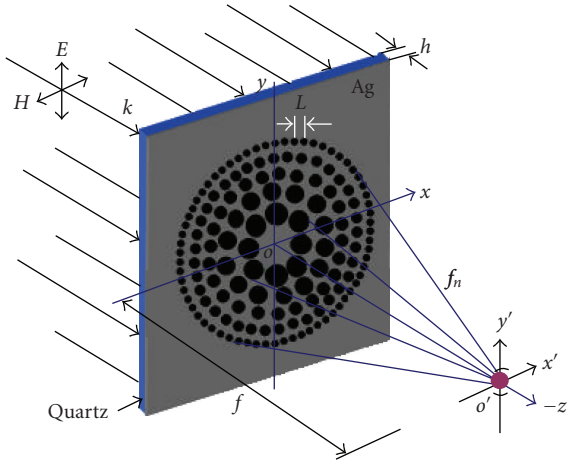

FIGURE 1: Schematic of the pinhole array with focal length f. Lateral central distance L determines wave coupling between the neighboring holes. The pinholes are uniformly distributed in the zones. It is illuminated by a plane wave with 633 nm incident wavelength and p-polarization (transverse-magnetic field with components of E_x, H_y, and E_z). The Ag film has permittivity $\varepsilon = -17.6235 + 0.4204i$ at $\lambda_0 = 633$ nm. The perfectly matched layer (PML) boundary condition was applied at the grid boundaries in the 3D FDTD simulation.

of $E_\perp$ field, an even larger increase in the cut-off condition is observed by considering a coupled localized surface plasmon polaritons (SPPs) wave propagating along y direction due to the longitudinal nature of the surface plasmon field inside the Ag film, in which the excitation light must have a component of the electric field parallel to the direction of the SPPs propagation or perpendicular to a surface. This leads to the cut-off wavelength effect intensifying as the pinhole diameters become smaller. The cut-off wavelength λc for the $E_\perp$ field illumination can be calculated by [12]

$$\tanh\left(\sqrt{\beta_{E_\perp^2} - k_0^2\varepsilon_{\text{air}}}\,\frac{d}{2}\right) = \frac{-\varepsilon_{\text{air}}}{\varepsilon_m}\frac{\sqrt{\beta_{E_\perp^2} - k_0^2\varepsilon_m}}{\sqrt{\beta_{E_\perp^2} - k_0^2\varepsilon_{\text{air}}}}, \quad (1)$$

where ε_m is the relative permittivity of the metal, ε_{air} is the relative permittivity of air, d is the diameter of the pinholes, and $k_0 = 2\pi/\lambda$ is the free-space wave vector. The other factor influences the transmission is $\delta = L/d$, where L is the central distance of the adjacent holes or periodicity of the pinholes along the same zone, as shown in Figure 1. We highlight this issue in this letter to analyze its influence on transmission and focusing. The cut-off wavelength effect occurs when the propagation constant is zero.

We selected a set of parameters arbitrarily to illustrate the working performance of the proposed structure. For instance, we designed a superlens for the purpose of focusing and imaging. The structure consists of 8 rings of pinholes with the following diameters (see inset pattern in Figure 2(a)): 158 nm (8th ring), 177 nm (7th ring), 202 nm (6th ring), 234 nm (5th ring), 280 nm (4th ring), 349 nm (3rd ring), 467 nm (2nd ring), and 735 nm (1st ring). For the wavelength $\lambda_{\text{in}} = 633$ nm at normal incidence, the pinhole diameters at the outer four rings are less than $\lambda/2$. The total dimension of the structure is 12.07 μm. All the pinholes have a fixed ratio $K = d/w = 3.0$, where d is the diameter of pinholes and w is the width of corresponding open zones in a zone plate.

In order to analyze the influence of δon the transmission and focusing, we chose $\delta = 1.25$, 1.5, 2.5, and 3.75 for three-dimensional (3D) electromagnetic (EM) field calculation using finite-difference and time-domain (FDTD) algorithm which is a powerful tool for modeling EM fields. Its basic principle is to discretize Maxwell's equations and sample continuous EM fields over a uniform space grid, and then obtain solutions for the fields in the time domain. Considerable CPU time (a total 6 hours running time for our 3D simulation) is required for obtaining the convergence of the simulation. In our FDTD 3D simulations, simulation time and mesh size are 150 fs $\Delta x = 20$ nm, $\Delta y = 20$ nm, and $\Delta z = 20$ nm, respectively (For the FDTD algorithm-based plasmonic effect study, it is better to set mesh size to less than 5 nm. However, our workstation with maximum memory size of 8 GB enables the 3D FDTD calculation with minimum mesh size of 20 nm only due to the large simulation area of 12 μm $\times$ 12 μm $\times$ 3.4 μm in x, y and z in our simulation. The lateral dimension is fixed by our design. Propagation distance of 2 μm after the exit plane in free space has to be defined due to the elongated focal length here.). For the materials in our structure with weak absorption, a long duration in the Fourier transform is required for obtaining a convergence of the EM fields [13, 14]. The normal incident light with the plane wave is employed for this example, as shown in Figure 1, for the illumination and propagation along z-direction. The incident wavelength of the light is in the visible regime ($\nu = c/\lambda_{\text{in}} = 474.34$ THz). The dielectric constant used for the Ag film at this wavelength is $\varepsilon = -17.6235 + 0.4204i$[16]. A silver film with thickness $h_{\text{Ag}} = 200$ nm has a microzone plate-like structure and the pinholes embedded in the film. Maxwell's equation is decoupled into the $E_\parallel$ and $E_\perp$ modes, as indicated in Figure 1. The $E_\parallel$ mode consists of E_y, H_x, and H_z field components. The $E_\perp$ mode consists of E_x, H_y, and E_z field components. Incident wavelength λ_{in} and δ of the superlens are used as the variable parameters to study the corresponding variations of the transmission and focusing performance.

For the pinholes with diameter $d < \lambda/2$, the propagation can still continue through them due to the localized SPPs wave coupling between the neighboring holes. The propagation length at an Ag/air interface is $L_{\text{SPP}} = 0.5/\beta'' = 428.5$ μm, where β'' is the imaginary part (phase change) of the propagation constant $\beta = \beta' + i\beta''$, and it is far larger than the pinhole central distance L. The nanoholes serve as point-like sources for the SPPs, whose constructive interference gives rise to focusing. This phenomenon was experimentally verified already by Yin et al. [16]. For $d > \lambda/2$, an interference between the SPPs wave and diffraction wavelets from the holes directly forms the focusing in free space. Here we highlight the influence of the cut-off wavelength effect on transmission property of the structure through the fixing pinholes diameter and changing the periodicity L of the pinholes only for the five outmost rings as the other pinholes diameter is larger than $\lambda/2$. The maximum intensity is observed for

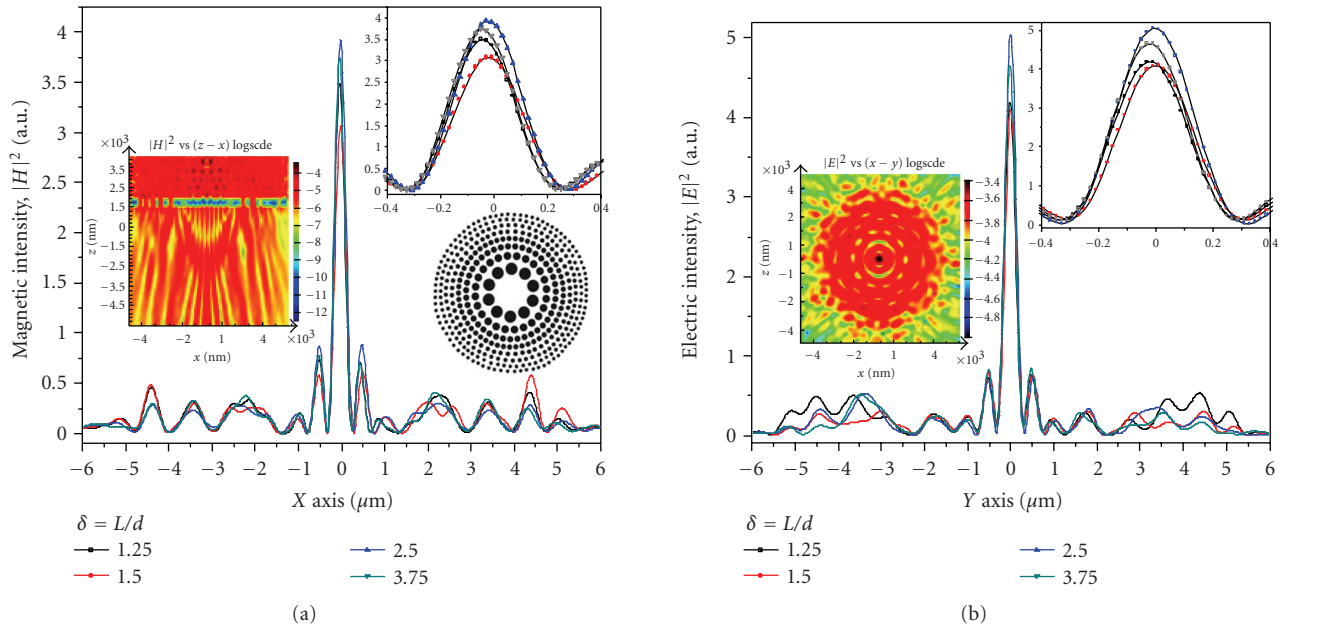

FIGURE 2: Results of electromagnetic field analysis for (a) H-field intensity $|H|^2$ distribution at x-z plane. Inset is 2D image of H-field intensity $|H|^2$ distribution at x-z plane for incident wavelength of 633 nm and layout of the pinhole structure. (b) E-field intensity $|E|^2$ distribution at y-z plane. Inset is 2D image of E-field intensity $|E|^2$ distribution at x-y plane.

the spots corresponding to first-order diffraction of the SPP Bloch wave. In contrast to the transmission without the SPPs excitation ($E_{\parallel}$ field), the field at the wavelengths of the enhanced transmission conditions has strong inhomogeneous components which are related to the surface polaritons [17]. Hence, no focusing appears there. For the transmission with the SPPs excitation ($E_{\perp}$ field), the electric intensity $|E|^2$ distribution at x-z plane and magnetic intensity $|H|^2$ distribution at y-z plane were calculated using the FDTD algorithm, respectively, as shown in Figure 2(a) and 2(b). It can be seen that an apparent focal region is observed for both components $|H|^2$ and $|E|^2$. Spot size at full-width and half-maximum (FWHM) increases slightly with the increase of the pinholes periodicity L. Figure 3 shows characteristics of the cut-off wavelength effect. It can be seen that redshift occurs with reducing the pinholes periodicity L. The observation is in agreement with the report in [18] and it may be attributed to the SPP coupling effect. The cut-off wavelength effect-related redshift is mediated by the SPPs coupling between the holes in y direction. The coupling is increased as L decreases. The sum of the SPPs wave on the top and bottom of the Ag film interferes with the diffraction wavelets from the larger pinholes, leading to the final focusing.

To further investigate focusing property of the superlens, the transmission and focusing in the free space after the exit plane of the Ag film are analyzed for different incident wavelengths ranging from 400 nm to 750 nm. Figure 4(a) and 4(b) shows components of $|H|^2$ distribution at x-z plane and $|E|^2$ distribution at y-z plane, respectively, for a structure with a fixed ratio $\delta = 1.25$. It can be seen that for the designed structure with the given dimension, the better focusing with beam spot size at FWHM beyond diffraction limit can be achieved

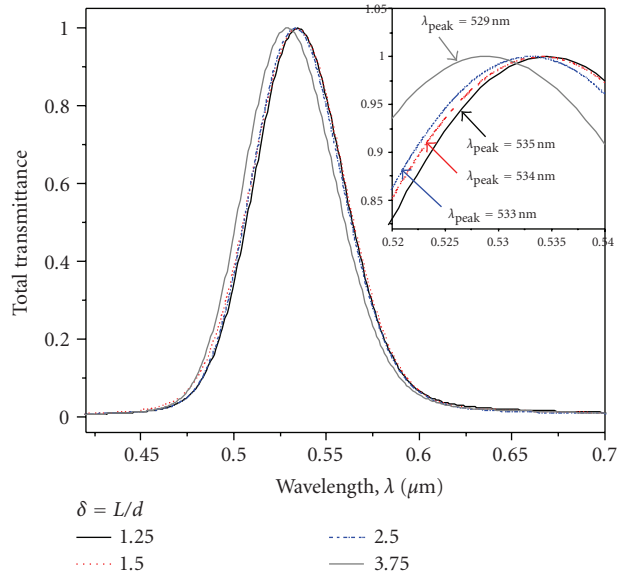

FIGURE 3: Plot of electromagnetic field transmission versus incident wavelength for different δratios ranging from 1.25 to 3.75. Redshift occurs with reducing pinhole periodicity L. The inset plot shows the central peak transmission.

for the wavelengths ranging from 400 nm to 530 nm. The intensity for both $|E|^2$ and $|H|^2$ decays significantly for longer wavelengths, especially for $\lambda_{in} = 750$ nm. The reason is that the number of cut-off wavelength caused nanopinholes increases as the incident wavelength increases. This leads to the pinholes at 3rd rings with diameters of 349 nm generating

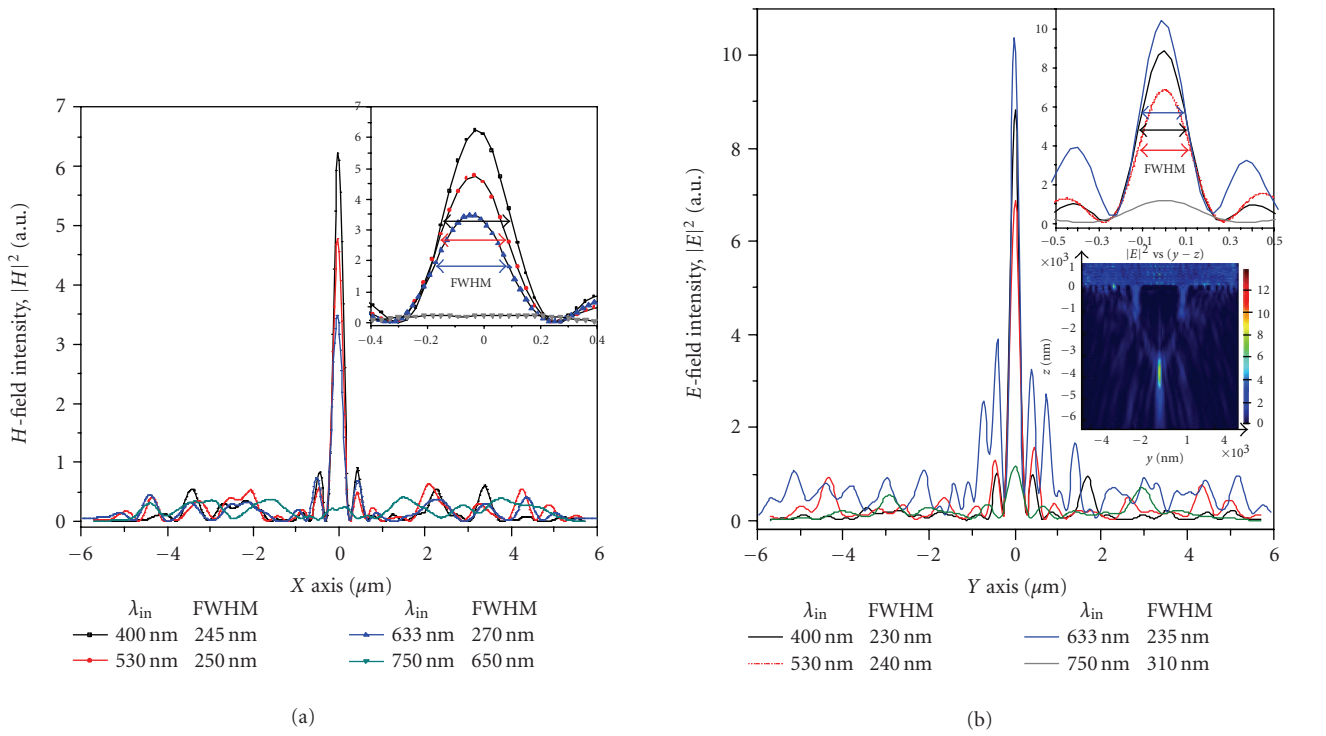

Figure 4: Results of electromagnetic field analysis of the designed nanopinhole-based plasmonic structure with fixed ratio $\delta = 1.25$ for different incident wavelengths. (a) H-field intensity $|H|^2$ distribution along x-axis. The inset plot of $|H|^2$ distribution at x-z plane shows the central transmission peaks. (b) E-field intensity $|E|^2$ distribution along y-axis. The central transmission peaks are shown more clearly in the inset plot of $|E|^2$ distribution at y-z plane for 400 nm incident wavelength. Inset 2D image is E-field intensity $|E|^2$ distribution at y-z plane.

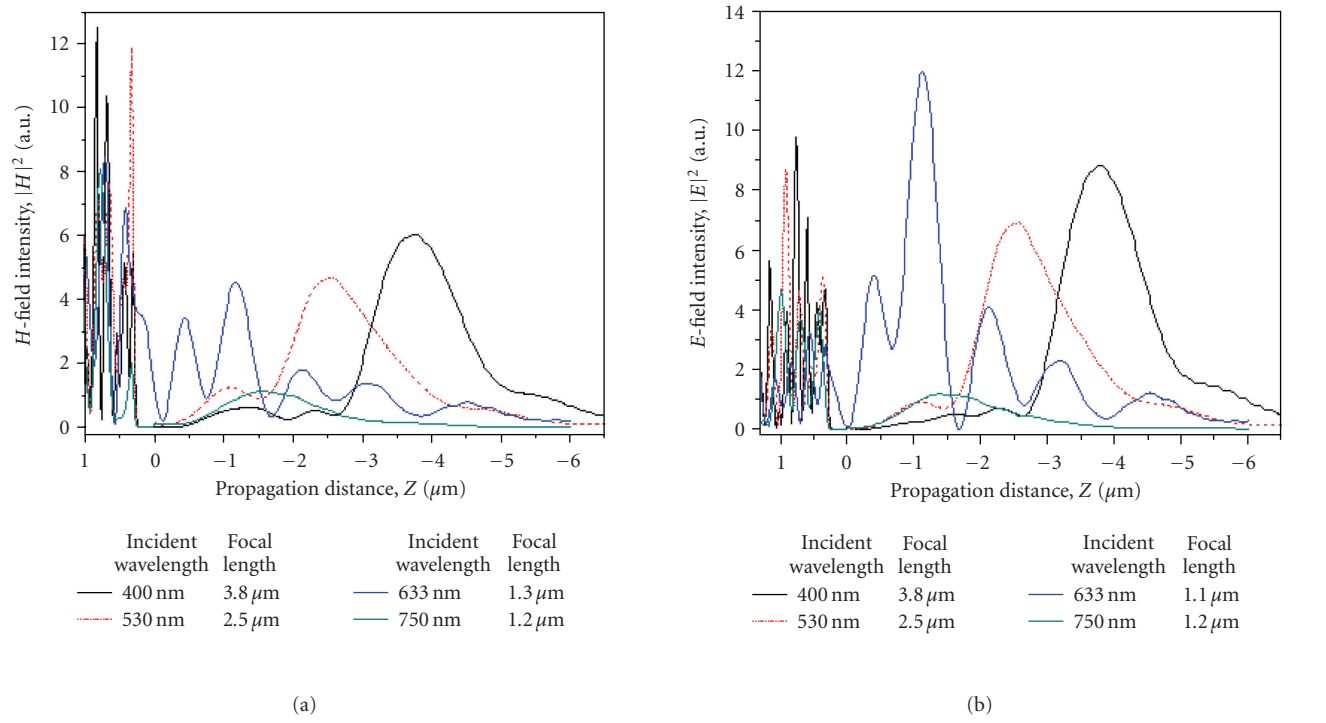

Figure 5: Results of electromagnetic field analysis for incident wavelength varying from 400 nm to 750 nm. (a) H-field intensity $|H|^2$ distribution versus propagation distance z. (b) E-field intensity $|E|^2$ distribution versus propagation distance.

the cut-off wavelength effect. However, they do not cause the cut-off wavelength effect for the shorter λ_{in} mentioned previously. The periodicity L of the pinholes distributed at these rings is fixed for the structure. Thus, increasing λ_{in} is equivalent to the case of reducing diameter of the pinholes in which cut-off wavelength effect will occur accordingly. Figures 5(a) and 5(b) shows the plot of EM field distribution versus propagation distance z for the different incident wavelengths. It can be seen that the maximum peak intensity appears at site of $z = -3.8\,\mu$m, $-2.5\,\mu$m, $-1.1\,\mu$m, and $-1.2\,\mu$m for the incident wavelength of 400 nm, 530 nm, 633 nm, and 750 nm, respectively. The number of transmission peaks as many as 5 appears for the 633 nm wavelength. It is possible to tune the system to keep fewer peaks or even one peak only by changing the incident wavelength to, for example, 400 nm or 530 nm.

In summary, a nanopinhole-based plasmonic nanostructure is put forth in this letter and the cut-off wavelength effect is addressed for analysis of transmission and focusing through the nanopinholes in near-field region. In a superlens with fixed pinhole diameters, propagation waves still exist for much reduced periodicity of pinholes due to the SPPs wave coupling, which interferes with the diffraction wavelets from the pinholes to form a focusing region in free space. Increasing incident wavelength is equivalent to reducing the pinhole diameters, and rapid decay of the EM field intensity will occur accordingly. The superlens proposed by us has the advantages of possessing micron-scale focal length and large depth of focus along the propagation direction. It should be especially noted that the structure of the superlens can be easily fabricated using the current nanofabrication techniques, for example, focused ion beam milling and e-beam lithography. It would be interesting to further explore applications of the nanopinhole-based plasmonic nanostructure for superfocusing and imaging with a spatial resolution beyond diffraction limit.

ACKNOWLEDGMENT

The authors would acknowledge the financial support from the 973 Program (Grant no. 2006CB302900) and the Chinese Nature Science Grants 60678035 and 60507014, and the financial support from Agency for Science, Technology and Research (A∗STAR), Singapore, through the project on "Novel Optical Nanoprobe for Nanometrology based on Surface Plasmon Polaritons." The authors also thank Mr. Haofei Shi for his helpful discussion regarding the relevant researches.

REFERENCES

[1] G. Schneider, "Cryo X-ray microscopy with high spatial resolution in amplitude and phase contrast," *Ultramicroscopy*, vol. 75, no. 2, pp. 85–104, 1998.

[2] W. B. Yun and M. R. Howells, "High-resolution Fresnel zone plates for x-ray applications by spatial-frequency multiplication," *Journal of the Optical Society of America A*, vol. 4, no. 1, p. 34, 1987.

[3] A. N. Kurokhtin and A. V. Popov, "Simulation of high-resolution x-ray zone plates," *Journal of the Optical Society of America A*, vol. 19, no. 2, pp. 315–324, 2002.

[4] L. Kipp, M. Skibowski, R. L. Johnson, et al., "Sharper images by focusing soft X-rays with photon sieves," *Nature*, vol. 414, no. 6860, pp. 184–188, 2001.

[5] A. V. Zayats and I. I. Smolyaninov, "Near-field photonics: surface plasmon polaritons and localized surface plasmons," *Journal of Optics A*, vol. 5, no. 4, pp. S16–S50, 2003.

[6] C. D. Pfeifer, L. D. Ferris, and W. M. Yen, "Optical image formation with a Fresnel zone plate using vacuum-ultraviolet radiation," *Journal of the Optical Society of America*, vol. 63, pp. 91–95, 1973.

[7] S. Cavalieri, L. Fini, E. Sali, and R. Buffa, "Enhancement of harmonic generation by Fresnel-lensing effects," *Optics Letters*, vol. 31, no. 9, pp. 1298–1300, 2006.

[8] A. N. Kurokhtin and A. V. Popov, "Simulation of high-resolution x-ray zone plates," *Journal of the Optical Society of America A*, vol. 19, no. 2, pp. 315–324, 2002.

[9] Q. Cao and J. Jahns, "Focusing analysis of the pinhole photon sieve: individual far-field model," *Journal of the Optical Society of America A*, vol. 19, no. 12, pp. 2387–2393, 2002.

[10] G. Andersen, "Large optical photon sieve," *Optics Letters*, vol. 30, no. 22, pp. 2976–2978, 2005.

[11] E. H. Anderson, V. Boegli, and L. P. Muray, "Electron beam lithography digital pattern generator and electronics for generalized curvilinear structures," *Journal of Vacuum Science & Technology B*, vol. 13, no. 6, pp. 2529–2534, 1995.

[12] R. Gordon and A. Brolo, "Increased cut-off wavelength for a subwavelength hole in a real metal," *Optics Express*, vol. 13, no. 6, pp. 1933–1938, 2005.

[13] C. Li, G. W. Kattawar, and P. Yang, "A new algorithm to achieve rapid field convergence in the frequency domain when using FDTD," *Journal of Electromagnetic Waves and Applications*, vol. 18, no. 6, pp. 797–807, 2004.

[14] W.-Y. Wu and C.-W. Kuo, "Novel FDTD algorithm with integration loop dependence," in *Proceedings of IEEE Antennas and Propagation Society International Symposium (APS '03)*, vol. 4, pp. 368–371, Columbus, Ohio, USA, June 2003.

[15] M. M. J. Treacy, "Dynamical diffraction explanation of the anomalous transmission of light through metallic gratings," *Physical Review B*, vol. 66, no. 19, Article ID 195105, 11 pages, 2002.

[16] L. Yin, V. K. Vlasko-Vlasov, J. Pearson, et al., "Subwavelength focusing and guiding of surface plasmons," *Nano Letters*, vol. 5, no. 7, pp. 1399–1402, 2005.

[17] L. Salomon, F. Grillot, A. V. Zayats, and F. de Fornel, "Near-field distribution of optical transmission of periodic subwavelength holes in a metal film," *Physical Review Letters*, vol. 86, no. 6, pp. 1110–1113, 2001.

[18] L. Martín-Moreno and F. J. García-Vidal, "Optical transmission through circular hole arrays in optically thick metal films," *Optics Express*, vol. 12, no. 16, pp. 3619–3628, 2004.